Available online at www.sciencedirect.com
ScienceDirect
Acta Materialia xxx (2006) xxx–xxx
Acta MATERIALIA
www.actamat-journals.com

Nanostructured coatings of glass fibers: Improvement of alkali resistance and mechanical properties

S.L. Gao, E. Mäder *, R. Plonka

Department of Composites, Leibniz Institute of Polymer Research Dresden, Hohe Strasse. 6, 01069 Dresden, Germany

Received 19 May 2006; received in revised form 20 September 2006; accepted 20 September 2006

Abstract

Surface defects cause the measured tensile strength of glass and other brittle materials to be significantly lower than their theoretical values. Coatings can be used to "heal" surface flaws and modify surface properties. Here, we describe an online process by which a nanometer-scale hybrid coating layer based on styrene–butadiene copolymer with multi-walled carbon nanotubes (MWCNTs) and/or nanoclays, as a mechanical enhancement and environmental barrier layer, is applied to alkali-resistant glass (ARG) and E-glass fibers. Our data indicate that the nanostructured and functionalized traditional glass fibers show significant improvements in both mechanical properties and environmental corrosion resistance. With low fractions of nanotubes (0.2 wt% in sizing), the strength of healed glass fiber increases by up to 70%. No apparent strength variation appears for nanoclay-coated fiber subjected to alkaline attack. The adsorption isotherms of moisture vapor on the fiber surface have been analyzed and an assessment of changes in the nanomechanical properties of the fiber surface is provided. It is shown that the sorption of moisture is reduced by the presence of nanoclay particles in the coating. We introduce a healing efficiency factor and conclude that the coating modulus, thickness and roughness are responsible for the mechanical improvement of fibers.

Keywords: Nanostructure; Coating; Surface defects; Corrosion; Glass fiber

1. Introduction

Surface defects of brittle materials cause the actual tensile strength to be much lower than the ultimate theoretical strength. Nanoscale surface defects provide extra stress at the tip of the cracks and can lead to stress-corrosion cracking at low stress levels, particularly in a humid environment. Polymer coatings are always applied to various fibers to protect them from mechanical damage during handling. Such coatings also act as a diffusion barrier to moisture reaching the fiber surface from the surrounding environment. Healing nanoscale surface flaws and enhancing a material's lifetime by coating, therefore, are important for many traditional materials in wide use in aggressive environments, such as glass fiber-reinforced concrete.

The recently developed surface-defect-free and high-purity carbon nanotubes have exceptional high Young's modulus and tensile strength. However, an effective utilization of their mechanical properties in composites is a longstanding problem. To date, the highest strength and Young's modulus reported in the literature are relatively disappointing: 1.8–3.2 GPa and ~40 GPa, respectively, for aligned nanotube composite bundles with very high-volume loading of nanotubes (60 wt%), which are a factor of 10 below those of the component individual nanotubes [1–3]. Even after very recent increases in fiber modulus of 120 GPa, the tensile strength of bundled nanotubes is limited to 116 MPa by the presence of localized defects and voids [4]. Therefore, finding an appropriate dispersion for the nanoreinforcements to increase volume concentration, limited by chemical inertness and van der Waals attractions, is not sufficient for producing high-quality materials.

* Corresponding author. Tel.: +49 351 4658 305; fax: +49 351 4658 284.
E-mail address: emaeder@ipfdd.de (E. Mäder).

1359-6454/$30.00 © 2006 Acta Materialia Inc. Published by Elsevier Ltd. All rights reserved.
doi:10.1016/j.actamat.2006.09.020

In contrast to the above "super-materials degraded by defects" approach, our recent work applied a "surface defects healed by super-materials" approach [5], because surface coatings can efficiently protect the fiber surface against alkali/acid/moisture and thus improve the fibers mechanical properties. Using less than 0.5 wt% nanotubes in coatings to heal common continuous glass fiber, strengthening by as much as 60% is achieved and no apparent variation in modulus appears. The mechanical properties of the healed glass fibers are equal to and even higher than the corresponding values of the aforementioned high-volume concentration-bundled nanotubes. From a statistical viewpoint, we found that the tensile strength of healed glass fibers can be well described by the bimodal Weibull cumulative distribution function, indicating that the failure is governed by different types of flaws [6]. The mechanical "healing" effect was viewed as the disappearance of severe surface flaws because of an increase of the crack tip radius, the flaw filled by coatings being elliptical rather than sharp [7]. Recent molecular dynamics simulations show that the stress concentration at the notch tip is significantly reduced due to the presence of the nanoparticles [8]. These results point to a simple means of fabricating systems that can self-heal, where nanoparticles dispersed in a polymer matrix can migrate to a crack generated at the interface between the polymer and a glassy layer [9]. Fundamentally, the optimized mechanical structure and nanostructured surface are motivated by the grace and efficiency of natural materials in a biomimetics approach. It is through the evolution of these materials, as shown in Fig. 1 (left), that multiscale structures (i.e. bones) and skin coverings with a flexible multilayer of overlapping tough scales (vertebrates, i.e. fishes) provide a protective layer against physical/chemical attack. The nanometer size of mineral particles, composed of insoluble protein keratin and minerals, ensures optimum strength and maximum tolerance of flaws [10]. As the structural size shrinks to the nanometer-scale, there is a transition in the fracture mechanism from the classical Griffith linear elastic fracture mechanics (LEFM) to one of homogeneous failure with no stress concentration at the crack tip, and the structure becomes insensitive to pre-existing flaws [11]. The surface free energy becomes more dominant and the material strength is limited by the theoretical strength of solid.

Coating is a widespread method of providing corrosion protection in order to improve the durability of engineering structures. Water is the major cause of swelling, loss of adhesion, deterioration of mechanical properties and the start of the corrosion process. We applied a styrene–butadiene coating on an ARG surface as an environmental barrier layer. This buffers the alkaline groups of the cementitious matrix and shows significantly improved corrosion resistance to alkali [12]. It was widely recognized that polymer–nanoclay composites, made by intercalating organophilic montmorillonite (MMT) to interpenetrating different polymer networks, have excellent barrier capability with significantly reduced permeability to moisture and gases [13,14]. The moisture permeability and diffusion behaviours of nanocomposites normally depend on the polymer type, nanoclay content, aspect ratio and degree of dispersion on silicate layers, as well as the interfacial adhesion. It was found that the water diffusivity in general

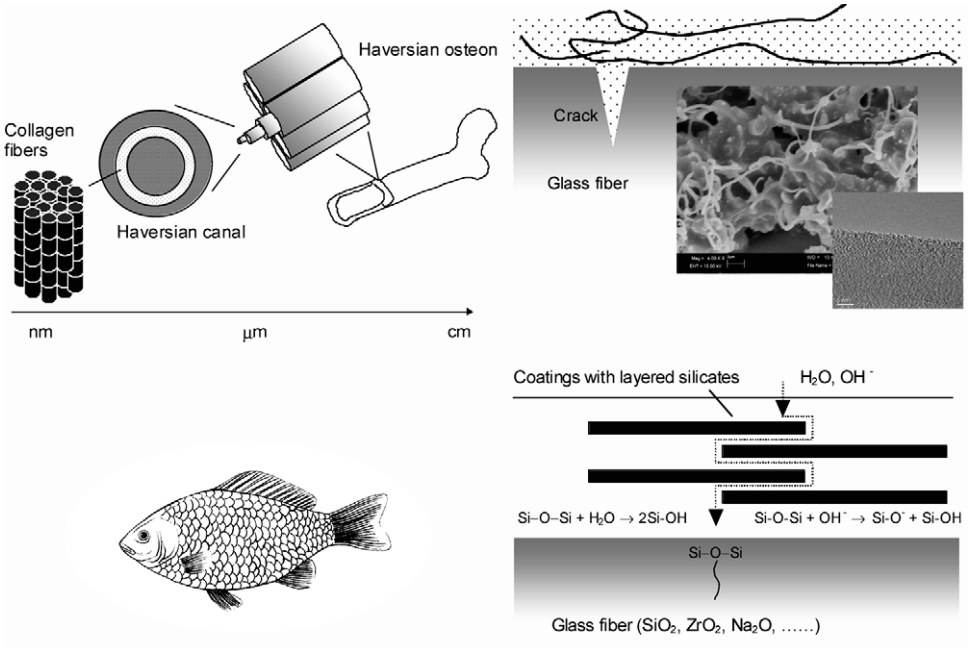

Fig. 1. Natural strategy of mechanical reinforcement and environmental resistance by multi-scale fibers and overlapping tough scales (left). Applications of nanostructured coatings with a nanotube/layered silicate polymer network were made onto a glass fiber surface to enhance the healing flaw effect and corrosion resistance (right). The inserts show the polymer/MWCNT network by SEM and the individual surface functionalized nanotube structure by TEM.

Please cite this article in press as: Gao SL et al., Nanostructured coatings of glass fibers: Improvement of ..., Acta Mater (2006), doi:10.1016/j.actamat.2006.09.020

decreased with increasing clay content and was reduced to half of its value in the neat vinylester resin with only 1 wt% of clay and the water absorption rate was reduced by about 40% for nanoclay–polyamide composites compared with the neat polymer [15]. A 50–80% decrease in water absorption was also reported for epoxy and poly(*s*-caprolactone) nanoclay composites [16,17]. A combined experimental and theoretical study of various poly(ethyleneoxide)- and poly(propylene oxide)-based compounds intercalated in montmorillonite and hectorite clays was studied and the diffusion coefficient of water molecules was reported as $4–32\times10^{-8}\,\mathrm{cm^2/s}$ [18,19]. To the best of our knowledge, the application of the moisture barrier properties of nanocomposite coating on glass fiber and the effect on the fiber's alkali-resistance are yet to be exploited.

To enhance surface environmental resistance and also heal nanoscale surface flaws, we report a hybrid approach for coatings systems (Fig. 1 right). The glass fibers are coated by differently functionalized layered clay silicates and/or multi-walled carbon nanotubes (MWCNTs) with nanostructured polymer. The application of nanocomposite coatings locally at the fiber surface could potentially yield both surface-defect-free and functionalized interfaces, which exhibit enhanced environmental durability as well as mechanical properties of fibers and composites.

2. Mechanical strengthening fiber with surface flaw by surface coatings

The critical flaw which limits the strength of fibers is in general located at the fiber surface; therefore, the fracture behaviour is strongly affected by the variation of coating properties. We developed a simple mechanical model based on Griffith fracture mechanics to roughly estimate the strength of coated fiber. Consider a smoothly coated fiber loaded in tension and having a thin circumferential crack, as shown in Fig. 2a. When the crack appears, the strain energy is released in a material volume adjacent to the crack. Assume that this volume comprises a conical ring whose generating lines are shown by broken lines and whose height is proportional to the crack length. On the other hand, the energy is consumed by the formation of new surfaces and deformation of coatings because of an elastic constraint. According to the energy balance, the coated fiber strength σ_f can be expressed as

$$\sigma_f > \bar{\sigma}_f = \sqrt{\frac{2\gamma E_f}{\left(\beta a^* - \frac{L(1+L/d)E_c}{E_f}\right)}} \tag{1}$$

where γ is the fracture surface energy and β is a constant coefficient of proportionality. E_f and E_c are Young's modulus of fiber and coatings, respectively. We used an apparent crack length a^* instead of a to take into account geometrical influences to surface defects arising from either coatings filling the crack tip or surface roughness. The flaw filled by coatings results in the possible reduction of apparent crack length, $a^* < a$. In contrast, a high surface roughness might make the apparent crack length larger, $a^* > a$, suggested by the calculated a^* value being proportional to the maximum height surface roughness of the fiber, R_{max} [6]. This implies that good levelling of coatings is a prerequisite for strengthening. Notably, the critical tensile stress of fiber with a surface flaw $\bar{\sigma}_f$ is significantly affected by the coating modulus and thickness. Accordingly, we introduce a nondimensional healing efficiency factor

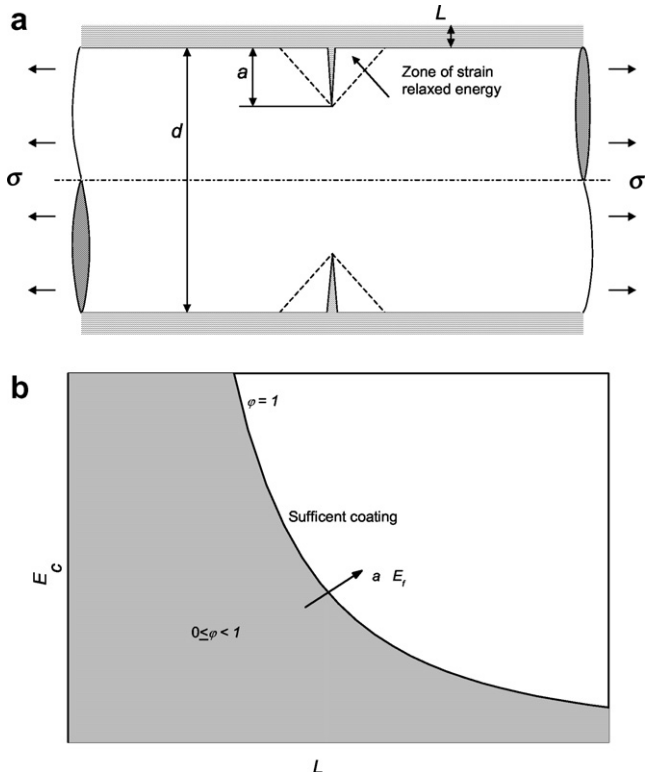

Fig. 2. (a) A sketch of a coated fiber with a surface flaw and (b) correlation of coating, flaw and fiber properties for efficient healing. The fiber is loaded in tensile stress σ and the circumferential surface flaw of length a serves as an initial crack. The fiber diameter and coating thickness are given by d and L, respectively, where a and L are much less than d.

$$\varphi = \frac{L(1+L/d)E_c}{\beta a^* E_f} \tag{2}$$

as an indication of whether the fiber is sufficiently coated and how the reinforcement effect is degraded by environmental corrosion. Therefore, the strength improvement ratio η can be related to a healing efficiency factor φ as

$$\eta = \frac{\sigma_f - \sigma_o}{\sigma_o} = \frac{1}{\sqrt{1-\varphi}} - 1 \tag{3}$$

where $\sigma_o = (2\gamma E_f/\beta a^*)^{1/2}$ is the strength of fiber without coatings. More rigorous analysis shows that, by reducing a^* to the equilibrium interatomic distance a_o of atoms at a force equal to zero, σ_o approaches the ultimate theoretical strength of the fiber, $\sigma_{max} = E_f/2\pi$. The healing efficiency factor ranges from zero to one, representing conditions from a non-coating/poor healing case to an efficiently healing case (Fig. 2b). Specifically, the thicker the

Please cite this article in press as: Gao SL et al., Nanostructured coatings of glass fibers: Improvement of ..., Acta Mater (2006), doi:10.1016/j.actamat.2006.09.020

coating layer and larger the stiffness of coatings the higher is φ and the tensile strength of fiber. On the other hand, the larger the size of defect and higher the stiffness of the fiber (see the arrow in Fig. 2b) for effective repairing, the thicker and stiffer the coatings required. This implies that a higher strength can be achieved for a fiber with a surface defect when the healing efficiency factor is close to one.

3. Experimental

3.1. Samples

The control ARG fibers utilized in this work were made at our institute with diameter of 17 μm. During the continuous spinning process, the ARG fibers were sized in situ by an alkali-resistant sizing consisting of a silane coupling agent, γ-aminopropyl-triethoxysilane, in conjunction with film formers and nanoparticles in the aqueous sizing, namely S1. The 0.2 wt% surface functionalized MWCNTs (IFW, Germany) are dispersed in the epoxy film former-based sizing. We applied surface coatings to the control ARG using either two kinds of styrene–butadiene copolymers with different T_g values (C1) or a commercial self-cross-linking styrene–butadiene copolymer (C2). Similarly, E-glass fibers with diameters of 20–23 μm were also coated with less than 0.5 wt% nanotubes in the coatings. The organo-clay particles (Nanofil 15, Süd-Chemie AG, Moosburg, Germany) in maleic anhydride-grafted polypropylene with a size of about 60–130 nm are dispersed in the obtained solution. A quaternary ammonium surfactant and a non-ionic surface-active agent were added to the dispersion for homogeneous distribution of the constituents with or without 1 wt% nanoclay. This method benefits from its ambient temperature treatment and environmentally friendly deposition, in addition to chemical versatility. The total weight gain due to the coatings is 5.3 wt%, measured by pyrolysis (600 °C, 60 min) of the coated fibers. We extracted the fibers in selected highly concentrated aqueous alkaline solution (5 wt% NaOH, pH 14) at 20 °C for 7 days, which is the most aggressive and corrosive condition for the fiber surface [6].

3.2. Characterization of fiber surface properties and tensile strength

An atomic force microscope (AFM) (a Digital Instruments D3100, USA) was used as both a fiber surface morphology imaging tool and a nanoindentation device to evaluate the fiber surface mechanical properties. It allows for precise continuous and simultaneous measurements in the indentation load and penetration depth. The cantilever (ULTRASHARP NSC16/50, MikroMasch, Estonia) has a normal spring constant of 35 N/m, a tip cone angle of 20°, a radius of 5–10 nm and a modulus of 160 GPa to assure good imaging resolution and nanometer-scale indents. The topography of samples was studied in tapping mode. Specimens were prepared by fixing separate short fiber filaments on a steel plate, within a thin layer of pre-coated epoxy at the bottom side of the fiber.

The influence of the organo-clay particles in the coating on the moisture sorption of the fibers was studied using an electronic microbalance (IGA-002, supplied by Hiden Analytical, Warrington, UK). After transferring the fibers to the measurement reactor, the system is evacuated (10^{-6} mbar) for about 1 day by a turbo-molecular pump until a constant weight was achieved. The sample environment temperature is controlled by a thermo regulated water bath. The sorption chamber was maintained at 25 ± 0.01 °C. Then, water vapor pressure is increased in suitable increments until saturation is reached. At each step, the mass gain is measured as a function of time until equilibrium is established. The water content at equilibrium is used to build the adsorption and desorption isotherms. The adsorption isotherm was analyzed by means of the Dubinin–Astakhov (DA) [20] and Brunauer–Emmet–Teller (BET) [21] methods, using equations:

$$\text{DA } W = W_o \exp\left[-\left(\frac{RT\,In(P_o/P)}{A_e}\right)^n\right] \tag{4}$$

$$\text{BET } W = W_o \frac{C \times P/P_o}{(1-(P/P_o)) \times [1-(P/P_o)+C \times (P/P_o)]} \tag{5}$$

where W is the equilibrium moisture content (g/100 g dry fiber solids) and W_o is the monolayer value at the absolute temperature T (K). R is the universal gas constant (8.314 kJ/kg mol K). P/P_o is the relative pressure of moisture, A_e is a characteristic energy of adsorption and n is an equation parameter. C is a constant which is dependent on the interaction in the solid–water system.

The tensile strength of a single fiber was measured using the Fafegraph Mechanical testing device (Fa. Textechno) equipped with a 10 N force cell. The gauge length is 20 mm and the cross velocity is 10 mm/min under 65% relative humidity and 20 °C according to specification EN ISO 5079. Based on a vibration approach, the diameter of each selected fiber was calculated from the fineness value, which was measured with a Vibromat ME (Fa. Textechno) according to specifications EN ISO 53812 and ASTM D 1577. To verify the effect of surface properties on the statistical distribution of the fiber tensile strength, the cumulative fracture probability F was fitted by a single Weibull distribution model through the least squares method and the Weibull modulus m_o was calculated.

4. Results and discussion

4.1. Fiber surface topography and mechanical properties

We first examined whether the dispersed organoclay was intercalated or exfoliated in the coatings. Individual crystallites observed by AFM (Fig. 3a) display the lath-type morphology of hectorite, consisting of a layered structure of aluminum sandwiched between two layers of silicon. The measured height of individual particles is

Please cite this article in press as: Gao SL et al., Nanostructured coatings of glass fibers: Improvement of ..., Acta Mater (2006), doi:10.1016/j.actamat.2006.09.020

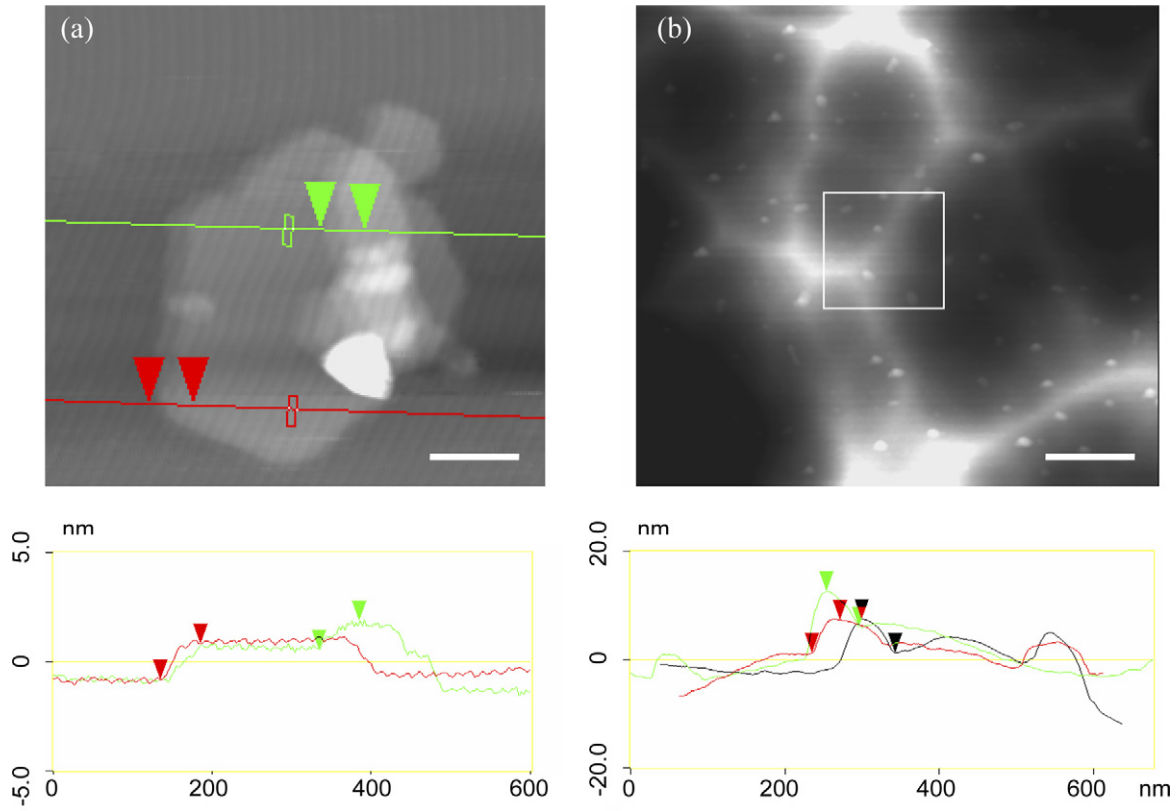

Fig. 3. AFM topography and section analysis (bottom) of (a) layered silicate clay and (b) the fracture surface of the coating with clay after alkali treatment. The distance between clay sheets is ~1.5 nm, shown by section profile of the individual clay sheet along the lines in the top view of the left figure. Scale bars represent (a) 100 nm and (b) 500 nm, respectively.

~1.5 nm, which corresponds to the distance between two single smectite layers. Fig. 3b shows that the fracture surface topography of coating film with clays after alkaline treatment consists of many similar-shaped particles. The measured thickness and lateral size of the particles are ~6 and ~80 nm, respectively, suggesting that the silicate layers of clay are intercalated. These clay platelets provide high surface areas of contact with the polymer matrix. The random distribution of the particles dispersed in the coating polymer matrix which are impermeable to molecular species and limit the diffusion of hydroxyl ions to glass surface and the crack tip is clearly visible. Obviously an appreciable level of platelet content and orientation is required to provide alkali barrier enhancement. Besides measuring the surface topography, images of other surface physical properties such as contact stiffness (hardness) and adhesion are measurable with the AFM. Fig. 4 shows the topography images and corresponding contact stiffness image of the pyrolysed fiber surface where the polymer was removed and clay particles remained. The stiffness images were determined by nanoindentation in force volume mode of AFM [22], in which an array of nanoindentation force–displacement curves were measured across the sample surface at regular intervals with a constant maximum indentation force. The stiffness map was plotted as a grey scale image, with lighter shades representing deeper indentation depth, in other words, lower contact stiffness. Worth noting is that no apparent difference of the stiffness and surface adhesion force was found between glass fiber and clay particles, which exhibit a very similar response to the indentation tip.

To understand the barrier levels that can be achieved with the nanometer-thin sheet-like layers of clay fillers in the coating, the sorption isotherms of fibers are presented in Fig. 5. The nanoclay-containing coating has lower values of both adsorption and desorption than the coating without clay at all ranges of relative pressure, particularly at high relative pressure, suggesting the clay coating adsorbed less water. All curves display the typical sigmoidal shape and exhibited low pressure hysteresis in all isotherms, which implies the coatings are typical materials in which restricted diffusion of the adsorbate, or swelling of the adsorbent, occurs.

To gain some qualitative insight into the physical significance of the clay performance, the applicability of the DA and BET equations over different regions of the isotherms was studied. The absorption data were analyzed by a nonlinear regression program as shown in Fig. 5b and c. The parameter values obtained are presented in Table 1. The accuracy of the description was estimated on the basis of the square correlation coefficient R^2. Both DA and BET methods show a good fit to the experimental data.

Please cite this article in press as: Gao SL et al., Nanostructured coatings of glass fibers: Improvement of ..., Acta Mater (2006), doi:10.1016/j.actamat.2006.09.020

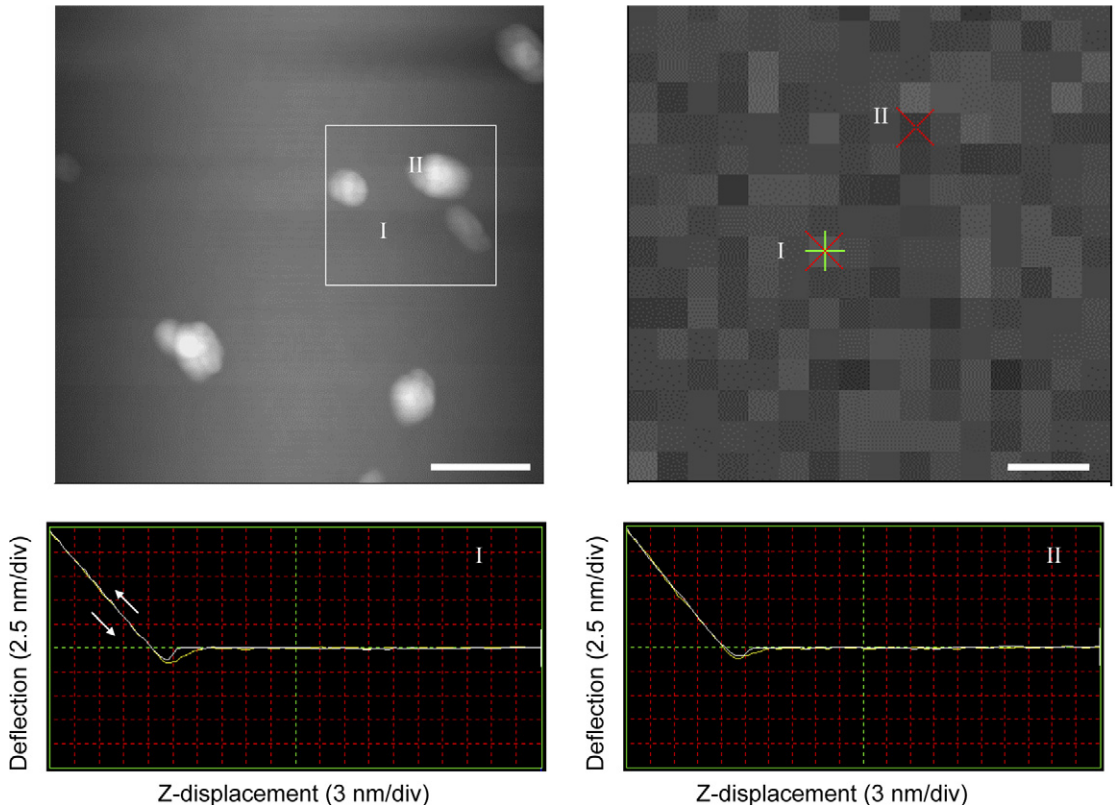

Fig. 4. AFM topography (left) and force volume image (right) in the square region of the clay on the fiber surface after pyrolysis treatment. Also shown are the cantilever deflection (force) vs. Z-displacement curves (bottom) corresponding to indentation at locations I and II on the fiber surface, respectively. Note the almost identical loading–unloading paths along the arrow directions, indicating the dominant elastic interaction between the indentation tip and the fiber/clay samples. Scale bars represent in the left figure 200 nm and in the right figure 50 nm, respectively.

Based on earlier works [23,24], the DA parameters qualitatively reflect the degree of heterogeneity (micropore volume and surface chemistry) of the materials. A_e is an indirect measure of the pore volume: it decreases when the pore volume increases. We found a significant decrease of the characteristic energy of adsorption A_e for coating with nanoclay, listed in Table 1. The increased pore volume can be attributed to the large clay–clay and clay–polymer interface areas. Additionally, these layered clay minerals can swell or shrink under the influence of changing relative humidity, temperature and external pressure [25].

The BET equation is based on adsorption on free surface without capillary condensation and therefore is applicable to adsorption for the mono- and multi-layer regions of the isotherm. In other words, the BET equation assumes energetically homogeneous surfaces. The fiber with nanoclay coatings, on the other hand, is heterogeneous but the adsorbing surface could be constructed as practically homogeneous up to a certain relative pressure. The constant C is related to heats of adsorption, which is dependent on the reaction in the water-coating systems. The higher C value for the sample with nanoclay showed that water is more strongly bound to the coating. This might be associated with the clay platelets and the interfaces adsorbing and retaining water molecules, because the cations are most often close to the clay surface and are then trapped within stable energetic wells [19]. Thus, the diffusion through the clay-loaded coating would appear much more slowly. In addition, the maximum concentrations of bound monolayer water in the coating, associated with the W_o values, are 4.1% and 2.3% for the coatings with and without nanoclay, respectively. The data further suggest that the moisture solvent uptake and concentration decrease accordingly when the organoclay is dispersed in the coating polymer.

To determine how the fiber surface morphologies are altered by the concentrated alkaline environmental attacks, we investigated fiber surface morphology and stiffness on a nanometer level (Fig. 6). The fairly smooth and featureless surface of the control (unsized) sample presents no apparent height differences (Fig. 6a), while the coated fibers with or without clay show the thin and thick coating layers with irregular distribution in all three dimensions (Fig. 6b and c). It is interesting to note that the coated fibers with nanoclay have similar surface features before and after extraction. In contrast, the coated fibers without clay after extraction had a microrough porous surface morphology with particles covering the surface, which is similar to the control sample. It seems that not only most of the coatings are removed but also the topmost layer of glass is chemically corroded.

It is well known that the chemical durability of silicate glass can be degraded in low or high pH aqueous solutions.

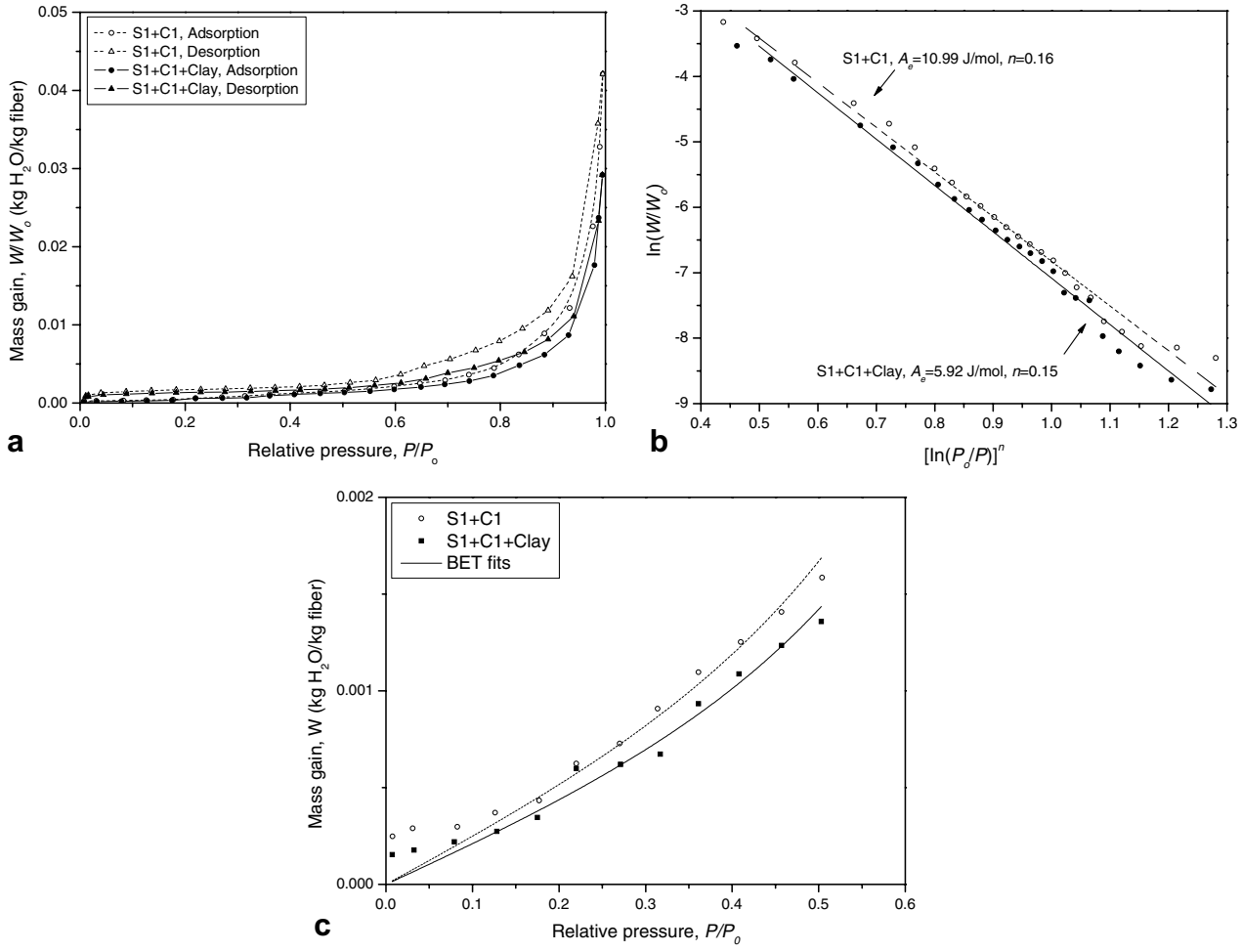

Fig. 5. Sorption isotherms of moisture vapour on sized glass fibers. (a) Adsorption–desorption isotherms, and adsorption isotherms fitted by (b) DA and (c) BET equations.

Table 1
Coefficients in the DA and BET equations

Sample	DA		BET		R^2
	A_e (J/mol)	n	W_o	C	DA/BET
S1 + C1	10.99	0.156	0.041	0.060	0.989/0.946
S1 + C1 + clay	5.92	0.151	0.023	0.089	0.990/0.968

The corrosion involved different mechanisms, such as ion exchange and congruent dissolution. The ion exchange or de-alkalization is attributed to highly mobile ions in the glass exchanging with hydrogen ion from water or vapour. Consider water that condenses on a glass fiber surface which leaches the alkali (sodium or potassium et al.) out of the glass:

$$\equiv Si{-}O^{-}Na^{+} + H_3O^{+} \rightarrow Si{-}OH^{-} + H_2O + Na^{+}$$

This process leaves behind a leached layer, termed silica gel, on the surface of the glass. The solution in the glass surface contains alkali, which increases the localized pH (>9) value. The solution in turn attacks glass network bonds, a process termed congruent dissolution, resulting in significant glass network dissolution and constituents going into solution:

$$\equiv Si{-}O{-}Si\equiv + OH^{-} \rightarrow \equiv Si{-}OH + \equiv Si{-}O^{-}$$

These two corrosion processes result in a number of pits/flaws appear on the fiber surface. By and large, the increased surface roughness and lengthened crack weaken the mechanical properties of the fiber [6].

Our nanoindentation tests provide an indication of the variability of the local contact stiffness of the fiber surface (see Fig. 6f). It is evident that surface stiffness within the indentation depth (<6 nm) was strongly affected by alkali extraction and the nature of the coating. We plotted the best-fit lines of experimental data in Fig. 6f, giving the surface modulus of 8 GPa for the fiber with nanoclay coatings. After alkaline treatment of the samples with coatings and nanoclay coatings, however, the surface moduli either increase to 31 GPa or decrease to 4 GPa, respectively. In conjunction with the above topographic imaging observation in the case of fiber with coatings (Fig. 6b), the increase of surface stiffness (modulus), which is very close to that of the control one, provides additional evidence of the organic

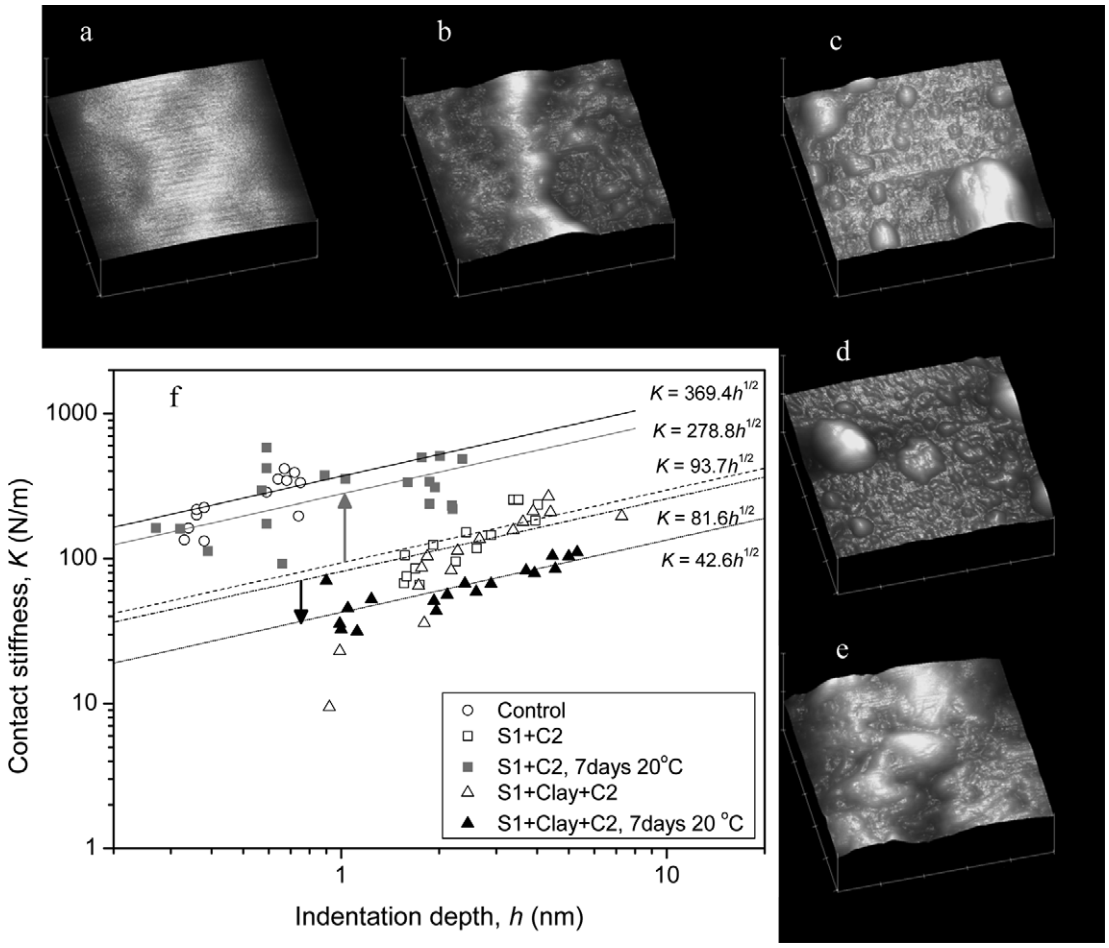

Fig. 6. AFM topography images (x, $y = 1$ μm, $z = 200$ nm) and surface stiffness of ARG. Fiber surfaces of (a) control, (b) coatings, (c) nanoclay coatings, (d) coatings after alkaline treatment and (e) nanoclay coatings after alkaline treatment. (f) AFM determination of contact stiffness vs. indentation depth for the silicon tip on the fiber surfaces. Variations of the nanoscale surface properties subjected to alkali attack are indicated by the arrows. The contact stiffness, K, is the slope of the initial elastic unloading curve of the nanoindentation test. As a quantitative evaluation of the contact stiffness and modulus of samples, the lines are the best-fit to a formalism [26] based on modified equation of Snedden, $K = 2\sqrt{2Rh}\cdot E_i E_s/\left[E_s(1-v_i^2)+E_i(1-v_s^2)\right]$, where R is the radius of curvature of the indenter tip and v is Poisson's ratio. E_s and E_i are Young's moduli of the specimen and the indenter, respectively.

layer being mostly removed. Because the constituents on the glass surface (SiO_2, ZrO_2, TiO_2, K_2O, etc.) enable different resistances to corrosion by alkaline solutions, a heterogeneous and porous surface structure appears and indentation data show a large amount of scatter. The reverse is true in the case of fiber with nanoclay coatings, where the modulus of the alkali-treated sample is apparently reduced. This is expected because of chemical corrosion or swelling more or less occurring in the remaining polymer coatings with the clay layer.

Overall, the clay-reinforced coating layer is rather alkali-resistant because of different physico-chemical mechanisms. A number of experimental and theoretical studies of polymer film with clay have shown that intrinsic permeability decreased significantly, i.e. the water diffusivity was reduced to half of its value in the neat polymer. It should be noted that, in general, the approximate values of diffusion coefficients of free cations or anions are 10^{-5} cm^2/s in water, 10^{-8} cm^2/s in the polymer and 10^{-12}–10^{-14} cm^2/s in the glass surface, respectively. The diffusion coefficient in the polymer coating with or without clay might not approach the value of the glass. Since a transport barrier layer affects both diffusion and sorption, a proposed mechanism of the improved alkali-resistance is that the clay particles retain water molecules and reduce the moisture adsorption and concentration in the coating layer and coating/fiber interface. The clay particles also act as obstacles, forcing both outside solution molecules and inside dissolved alkali ions to diffuse via long detours round the platelets. In other words, the congruent dissolution process was slowed down by the nanoclay coating through the control of advection, sorption and diffusion behaviour. Additionally, taking into consideration the chemical effects of the coating, as revealed by zeta-potential measurements in our early work [12], the acidic groups (i.e. COOH) of coating polymer were dominant on the fiber surface before and after NaOH treatment. Since the congruent dissolution of the corrosion process is only valid in a high pH environment, the coating with an acidic character, as an alkali-deficient layer, can slow down the deterioration

process by limiting the increase of the localized pH value and the growth of the silica gel layer.

4.2. Fiber mechanical properties

We next then investigated the tensile performance of the single fibers with either nanotubes or an organoclay surface nanostructured ARG. Fig. 7a shows that the tensile strength values are significantly improved for all systems. The fiber strength increased by 25% at an organoclay loading of 1 wt%. Importantly, the fiber strength increased by up to 70% at an MWCNTs loading of only 0.2 wt% in the sizings. Interestingly, as shown in Fig. 7b, both the Weibull plot lines and the Weibull modulus m_o of the coated systems shift to higher values than those of the control. This indicates that the strength-controlling surface defects have a lower-heterogeneity distribution and the size of the defects is reduced. In other words, the healed flaws on the coated fibers show similar flaw size, severity and homogeneity relative to those on the control fibers.

The effects of alkaline attacks on the average fiber strength are compared in Fig. 7a. It is evident that samples of clay coatings would not yield a significant strength reduction upon treatment. By contrast, a significant strength reduction occurred for systems with nanotube sizings. This can be partly compensated for by an additional styrene–butadiene coating with carboxyl radicals, which causes an enhanced alkali-resistance as confirmed by the marginal strength reduction. Nevertheless, the coated fibers have higher strength values than the control after alkaline corrosion, reflecting the improved environmental durability for fibers with nanostructured coatings.

Fig. 7c shows the remarkable mechanical strength improvement for both ARG and E-glass fibers with nanotube coatings, corresponding to the highest healing efficiency factor. Moreover, the variation of healing efficiency factor indicates how strong the resistance of the coatings subjected to environmental attack is. For example, there is no significant reduction of φ for fiber with nanoclay coatings after alkaline treatment, which repre-

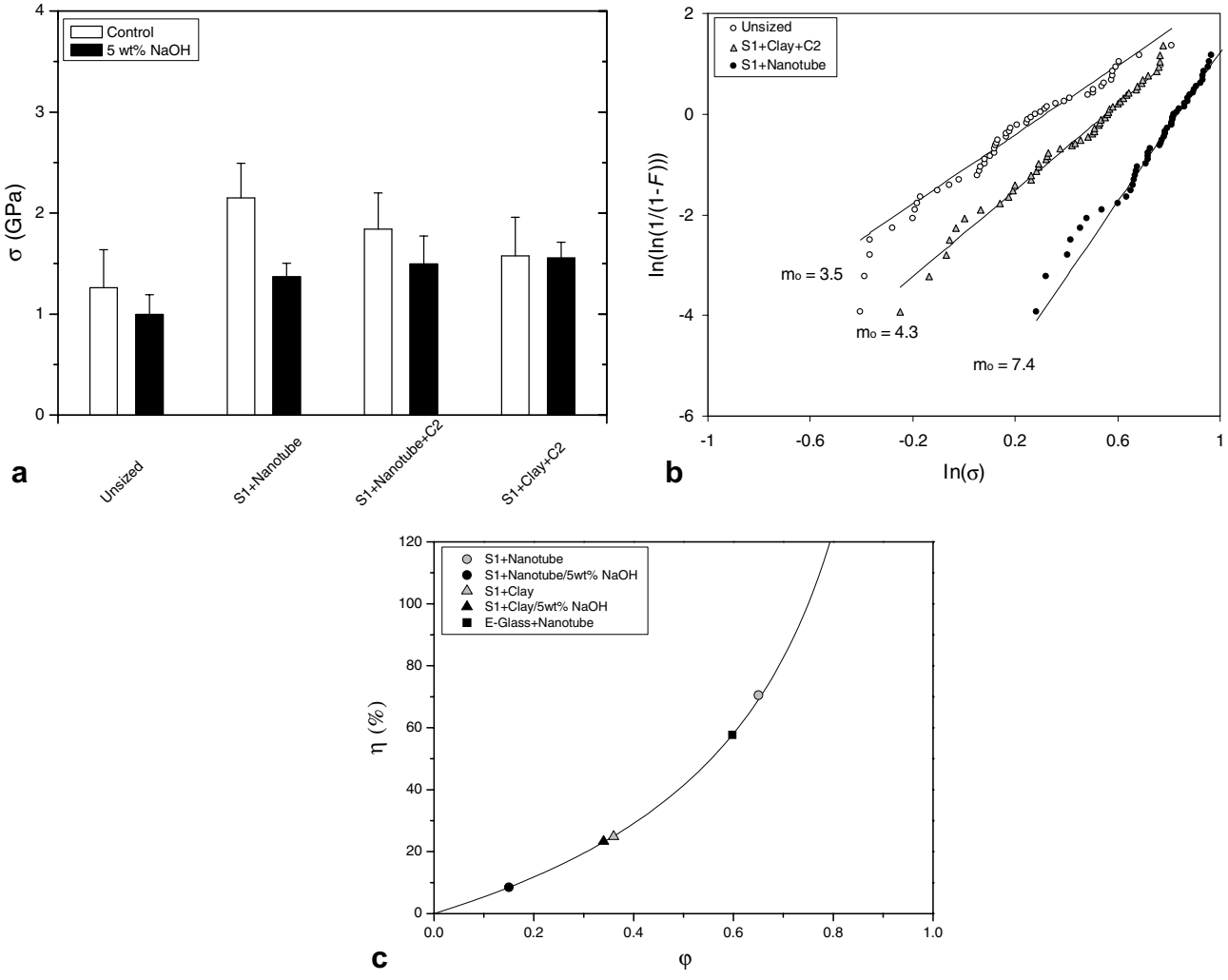

Fig. 7. Dependence of the mechanical properties and corrosion resistance on ARG surface coatings: (a) Effect of the nanostructured coatings with low fraction nanoreinforcements on the tensile strength of ARG before and after alkaline treatment. (b) Weibull plots of fiber fracture probability. (c) Response of the strength variation ratio to the healing efficiency factor. Error bars represent standard deviations.

Please cite this article in press as: Gao SL et al., Nanostructured coatings of glass fibers: Improvement of ..., Acta Mater (2006), doi:10.1016/j.actamat.2006.09.020

sents its high environmental barrier and anti-corrosion property. Finally, the coating Young's modulus can be estimated based on the tensile strength of the fiber as

$$E_c = \frac{2\gamma E_f^2}{L(1+L/d)}\left(\frac{1}{\sigma_o^2}-\frac{1}{\sigma_f^2}\right) \quad (6)$$

Taking $E_f = 70$ GPa, $\gamma = 1.75$ J/m^2 for glass [27], and an average $L = 600$ nm for the coatings, we can calculate E_c to be ~9 GPa for nanotube coatings and ~6 GPa for clay coatings, respectively, a fairly good agreement with the aforementioned coating modulus measured by nanoindentation. Because the rough calculation does not take into account possible plastic deformation/interfacial failure, the moduli are likely to be overestimated. They are reasonably consistent with the calculated theoretical values of the two corresponding nanocomposite coatings by rule of mixture, which are 5 and 3 GPa, respectively.

Potential mechanisms of the mechanical property improvement include the contributions of different factors. Firstly, as aforementioned, the coating layer and organosilicate plates prevent moisture/alkali contact and reaction with glass lattice at a crack tip (stress corrosion). The acidic groups (i.e. COOH) of the coating molecule interact with or absorb free cations and anions from the environment, leading to a slowdown of the corrosion process. Secondly, the coatings and the nanotube's "bridging" effect and interface debonding/plastic deformation around the crack tip cause redistribution of stress and crack stopping. Thirdly, compressive stress on the fiber surface might prevent crack opening/propagation by the shrinkage of polymer solidification. This is similar to the reinforcement mechanism based on ion exchange [28], where high compressive stresses are generated in the fiber surface by replacing the ions in the surface layer with larger ions, thereby impeding the initiation of cracks in tensile areas. Overall, nanostructuring coatings show promising potential in nanodefect repair and surface functionalization for different applications.

5. Summary

An experimental investigation of nanocomposite coatings for improving alkali-resistance and healing surface flaws of glass fibers was performed. We found that, with a low fraction of nanoreinforcements, the nanostructured and functionalized traditional glass fibers show significant improvement in both environmental corrosion resistance and mechanical properties. The moisture solvent uptake and concentration decrease when the organoclay is dispersed within the coating polymer. The surface contact stiffness of the styrene–butadiene-coated fibers with nanoclay exhibits similar values before and after alkali attack, while the contact stiffness of the control ARG significantly decreases after the treatments. The clay-reinforced coating layer is rather alkali-resistant, leading to a slowdown of the corrosion process because of both physical and chemical mechanisms. The remarkable mechanical strength improvement is found for both ARG and E-glass fibers with nanotube coatings, corresponding to the highest healing efficiency factor.

Acknowledgements

This work was supported by the German Research Foundation (DFG) within the Collaborative Research Centre "Textile Reinforcement for Structural Strengthening and Retrofitting (SFB528)". The authors wish to thank Werner Ehrentraut, Ruth Preisker, Jian Wen Liu, Rong Chuan Zhuang, Bianka Pusch and Dr. Victoria Albrecht for experimental assistance and helpful discussions.

References

[1] Vigolo B, Penicaud A, Coulon C, Sauder C, Pailler R, Journet C, et al. Science 2000;290:1331–4.
[2] Vigolo B, Poulin P, Lucas M, Launois P, Bernier P. Appl Phys Lett 2002;81:1210–2.
[3] Dalton AB, Collins S, Razal J, Munoz E, Ebron VH, Kim BG, et al. J Mater Chem 2004;14:1–3.
[4] Ericson LM, Fan H, Peng H, Davis VA, Zhou W, Sulpizio J, et al. Science 2004;305:1447–50.
[5] Gao SL, Mäder E, Plonka R, Liu JW. Surface flaw sensitivity of glass fibers with nano-reinforcement in polymer coating. In: Verijenko VE, Adali S, Morozov E, Klemperer CJ, editors. Proceedings of the 15th international conference in composite materials (ICCM-15), Durban, South Africa; 2005, [CD-ROM], p. 1–10, ISBN:1-86840-589-3.
[6] Gao SL, Mäder E, Abdkader A, Offermann P. Langmuir 2003;19:2496–506.
[7] Zinck P, Mäder E, Gerard JF. J Mater Sci 2001;36:1–8.
[8] Tyagi S, Lee JY, Buxton GA, Balazs AC. Macromolecules 2004;37:9160–8.
[9] Gupta S, Zhang QL, Emarick T, Balazs AC, Russell TP. Nature Mater 2006;5:229–33.
[10] Gao HJ, Ji BH, Jäger IL, Arzt D, Fratzl P. Proc Natl Acad Sci USA 2003;100:5597–600.
[11] Gao HJ, Ji BH. Eng Fract Mech 2003;70:1777–91.
[12] Gao SL, Mäder E, Plonka R. Acta Mater 2004;52:4745–55.
[13] Yano K, Usuki A, Okada A, Kurauchi T, Kamigaito O. J Polym Sci Part A 1993;31:2493–8.
[14] Lan T, Kaviratna PD, Pinnavaia TJ. Chem Mater 1994;6:573–5.
[15] Okada A, Kawasumi M, Usuki A, Kojima Y, Kurauchi T, Kamigaito O. Nylon 6-clay hybrid. Mater Res Soc Proc 1990;171:45–50.
[16] Kim JK, Hu C, WOO RSC, Sham ML. Compos Sci Technol 2005;65:805–13.
[17] Messersmith PB, Giannelis EP. J Appl Polym Sci 1995;33:1047–57.
[18] Hackett E, Manias E, Giannelis EP. Chem Mater 2000;12:2161–7.
[19] Boulet P, Bowden AA, Coveney PV, Whiting A. J Mater Chem 2003;13:2540–50.
[20] Dubinin MM. Progress in surface and membrane science, vol. 9. New York: Academic Press; 1975.
[21] Brunauer S, Emmett PH, Teller E. J Am Chem Soc 1938;60:309–12.
[22] Gao SL, Mäder E, Zhandarov S. Carbon 2004;25:515–29.
[23] Rand B. J Coll Interf Sci 1976;56:337.
[24] Ghosal R, Smith DM. J Porous Mater 1996;3:247–55.
[25] Tambach TJ, Bolhuis PG, Smit B. Angew Chem, Int Ed 2004;43:2650–2.
[26] Gao SL, Häßler R, Mäder E, Bahners T, Opwis K, Schollmeyer E. Appl Phys B 2005;81:681–90.
[27] Lawn BR. Fracture of brittle solids. 2nd ed. Cambridge: Cambridge University Press; 1993.
[28] Bartholomew RF. Ceramics and glasses. ASM Int 1991;4:460–3.